
Slimming Neural Networks using Adaptive Connectivity Scores

Madan Ravi Ganesh
EECS
University of Michigan
Ann Arbor, MI 48109

Dawsin Blanchard
SCIS
University of Maine
Orono, ME 04469

Jason J. Corso
EECS
University of Michigan
Ann Arbor, MI 48109

Salimeh Yasaei Sekeh
SCIS
University of Maine
Orono, ME 04469

Abstract

There are two broad approaches to deep neural network (DNN) pruning: 1) applying a deterministic constraint on the weight matrices, which takes advantage of their ease of implementation and the learned structures of the weight matrix, and 2) using a probabilistic framework aimed at maintaining the flow of information between layers, which leverages the connections between filters and their downstream impact. Each approach's advantage supplements the missing portions of the alternate approach yet no one has combined and fully capitalized on both of them. Further, there are some common practical issues that affect both, e.g., intense manual effort to analyze sensitivity and set the upper pruning limits of layers. In this work, we propose *Slimming Neural networks using Adaptive Connectivity Measures* (SNACS), as an algorithm that uses a probabilistic framework for compression while incorporating weight-based constraints at multiple levels to capitalize on both their strengths and overcome previous issues. We propose a hash-based estimator of *Adaptive Conditional Mutual Information* (ACMI) to evaluate the connectivity between filters of different layers, which includes a magnitude-based scaling criteria that leverages weight matrices. To reduce the amount of unnecessary manual effort required to set the upper pruning limit of different layers in a DNN we propose a set of operating constraints to help automatically set them. Further, we take extended advantage of weight matrices by defining a *sensitivity criteria* for filters that measures the strength of their contributions to the following layer and highlights critical filters that need to be protected from pruning. We show that our proposed approach is faster by over 17x the nearest comparable method and outperforms all existing pruning approaches on three standard Dataset-DNN benchmarks: CIFAR10-VGG16, CIFAR10-ResNet56 and ILSVRC2012-ResNet50.

1 Introduction

The challenge of obtaining near real-time performance, in domains like autonomous vehicle navigation [Bechtel et al., 2018, Fridman et al., 2017, Nurvitadhi et al., 2017] and simultaneous machine translation [Gu et al., 2017, Jia et al., 2019], constrained by the restricted availability of memory on hardware has brought increased attention to the field of deep neural network (DNN) pruning in recent years [Gale et al., 2019, Liu et al., 2018]. The main objective of pruning is to maintain an

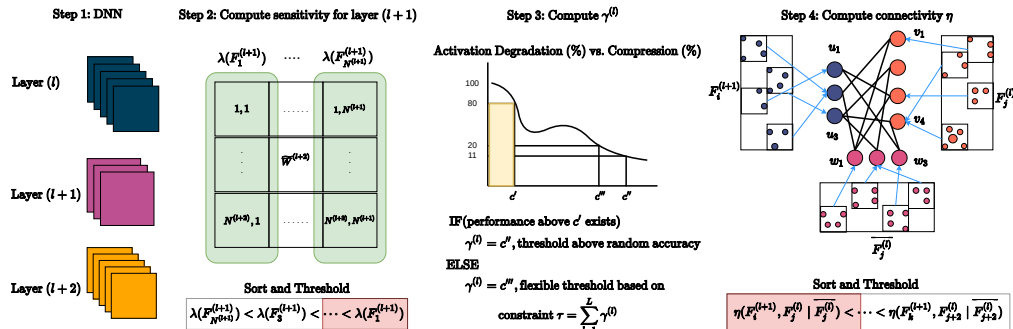


Figure 1: Illustration of the steps involved in pruning connections between layer l and $l + 1$. First, we compute the sensitivity of filters in $l + 1$ as the sum of normalized weights between filters in layer $l + 1$ and $l + 2$. We create a subset of relatively insensitive filters whose connections can be pruned. Then we use our set of operating constraints, based on the degradation of activation quality at various compression levels, to decide on the upper pruning limit for layer $l + 1$. Finally, we use the hash-based ACMI estimator to compute the connectivity scores between filters in layer l and $l + 1$ and threshold these scores to obtain our final pruned layer.

adequate level of performance, often within a few percent of the uncompressed DNN, while only using a fraction of the memory and FLOPs consumed by the uncompressed DNN.

While each of the two main approaches to pruning, deterministic constraints on weights matrices [Wen et al., 2016, Luo et al., 2017, Han et al., 2015] and probabilistic frameworks [Ganesh et al., 2020, Dai et al., 2018, Luo and Wu, 2017], have their individual benefits, deterministic constraints on weight matrices are simple to implement and use the learned underlying structure of weight matrices while probabilistic approaches focus on the connectivity between filters and their downstream impact, they individually contain weaknesses which can be solved by the alternate method. Yet, there has not been a recent work that combines both approaches and improves upon prior work. Also, there are some practical issues prevalent among both, e.g., the labor intensive cyclical process of analyzing the sensitivity of different layers in a DNN and imposing an upper limit on pruning for each layer.

To leverage the strengths of both the probabilistic framework for pruning and constraints on weight matrices as proxies for the importance of filters, we propose *Slimming Neural networks using Adaptive Connectivity Scores* (SNACS), Fig. 1. In SNACS, we introduce the *Adaptive Conditional Mutual Information* (ACMI) measure that uses the magnitude of weights as a scaling function within the probabilistic framework of conditional mutual information. The ACMI measure provides the connectivity scores between pairs of filters across adjacent layers in the entire DNN, which are then thresholded and used to prune weight matrices. In this work, we explore a multitude of scaling functions and highlight the improvement offered by weight matrix-based functions.

To remove the manual effort involved in setting the upper pruning limit of layers, we define a set of operating constraints to automatically set them. The rules are based on the degradation in quality of activations, measured using an SVM model, from different layers at various levels of compression. Additionally, we encapsulate the importance of a filter using our proposed *Sensitivity* criteria, defined as the sum of its contributions (normalized weights) to filters in the following layer. Using this measure, we curate a subset of relatively less sensitive filters that can be pruned based on their connectivity scores while we retain all the connections to highly sensitive filters. By using *Sensitivity* in conjunction with our set of constraints to define the upper pruning limit of layers, we can boost the overall compression (%) while maintaining accuracy.

2 Related Works

2.1 Deterministic Constraint Weight Matrix

Modification of Objective Function Inducing sparsity in weight matrices by modifying the objective function involves imposing a strong constraint on how weights develop during training. Constraints can range from single or multiple l_n norm constraints [Liu et al., 2017] on channel out-

puts, simple patterned masks to regulate group sparsity [Lebedev and Lempitsky, 2016], optimizing over group-lasso objective function [Wen et al., 2016], to more complicated balancing of individual vs. group sparsity constraints [Yoon and Hwang, 2017]. We do not compare against works that modify the objective function because they optimize over a fundamentally different constraint. Further, they contain multiple iterations of pruning, built-in to training while in our work we limit the number pruning and retraining steps to exactly one, after training is concluded.

Constraint on Weight Matrices One of the earliest works in pruning used the hessian between the objective function and weights of the network to compress the network [LeCun et al., 1990]. Since then, a number of advancements in the form of direct thresholds on weights [Han et al., 2015], l_1 constraint on the filters [Li et al., 2017], posing the removal of filters as an optimization objective [Luo et al., 2017] and using the reconstruction loss of features to derive the importance of weights [Yu et al., 2018] have been proposed. By virtue of how these methods are framed, they often do not account for downstream impact of pruning or are strongly dependent on the deterministic relationships between weights. Using a combination of magnitude-based scaling functions within a probabilistic framework for pruning, we overcome these issues.

2.2 Probabilistic Frameworks

More recently, information theory-based approaches measure the importance of a filter through the entropy of its activations [Luo and Wu, 2017], using the information bottleneck principle to minimize the redundancy between adjacent layers [Dai et al., 2018] and using a geometric conditional mutual information measure to determine the dependencies between filters pairs in adjacent layers [Ganesh et al., 2020]. Their core philosophy is to reduce redundancy while maintaining the flow of information between layers. In SNACS, we use a probabilistic framework for pruning which contains embedded constraints on the weight matrix, thus leveraging the value of both pruning approaches. By highlighting sensitive filters that need to remain un-pruned and automatically deciding on the upper pruning limit of layers we overcome some of the practical issues of previous methods.

3 SNACS: Design Details

3.1 Algorithm

Setup and Notations We assume that a DNN contains L layers where, we compute the connectivity (η) between filters in every adjacent pair of layers. The total number of filters in layer $(l + 1)$ is denoted by $N^{(l+1)}$. A lower value of l indicates that it is closer to input than the output layer. Activations from a filter are denoted by $F_i^{(l)} \in \mathbb{R}^{m \times 1}$, where i is the index of a filter and m is the number of samples. The final dimension of activations are averaged into a scalar value. The set of activations from filters in layer l , excluding $F_i^{(l)}$, are given by $\overline{F_i^{(l)}}$. There are two typical constraints applied for pruning in SNACS, δ over the connectivity scores, $\eta(\cdot)$, between filters (Section 3.2), and $\gamma^{(l+1)}$ which defines the upper pruning percentage for layer $l + 1$ (Section 3.3). Based on our pruning criteria, the set of filter connections for $F_i^{(l+1)}$ that are retained are stored in set $S_{F_i^{(l+1)}}$.

Algorithm 1: SNACS pruning between filters of layers $(l, l + 1)$

```

for Every pair of layers  $(l, l + 1), l \in 1, 2, \dots, L - 1$  do
  Initialize  $S_{F_i^{(l+1)}} = \text{INSENSITIVE\_FILTERS}(\{1, 2, \dots, N^{(l+1)}\})$ ;
  for  $F_i^{(l+1)}, i \in \text{INSENSITIVE\_FILTERS}(\{1, 2, \dots, N^{(l+1)}\})$  do
    for  $F_j^{(l)}, j \in 1, 2, \dots, N^{(l)}$  do
      Compute  $\eta(F_i^{(l+1)}, \overline{F_j^{(l)}})$ ;
      if  $\eta(F_i^{(l+1)}, \overline{F_j^{(l)}}) \leq \delta$  and  $|S_{F_i^{(l+1)}}|/N^{(l+1)} \leq (\gamma^{(l+1)})$  then
         $S_{F_i^{(l+1)}} = S_{F_i^{(l+1)}} \setminus F_j^{(l)}$ 
      end
    end
  end
end

```

Description The overall goal of the algorithm is to find the set of filters that contribute a majority of information between layers and retain their values in the weight matrix. We apply SNACS between adjacent layers of a DNN where, first, we identify a subset of relatively insensitive filters

in $l + 1$ that can be pruned. $S_{F_i^{(l+1)}}$ is initialized as these subset of filters. Then, we compute the connectivity, η , between activations from every filter in layer l and the subset of filters in $l + 1$ using our proposed hash-based ACMI estimator. The connectivity score evaluates the strength of the relationship between two filters in the context of contributions from all the filters from layer l . Finally, if the connectivity score is lower than a threshold level δ , and the number of pruned filters do not exceed the pre-determined upper limit, denoted by $\gamma^{(l+1)}$, we remove the index of the filter from $S_{F_i^{(l+1)}}$. The weights for retained filters/neurons are untouched while the weights for the entire kernel/elements are zeroed out for pruned filters/neurons. While Algorithm 1 can be applied to each filter individually, we apply it to groups of filters to improve run-time performance. We define $G^{(l+1)}$ as the total number of groups in layer $l + 1$, where a group of filters is selected sequentially.

3.2 Adaptive Conditional Mutual Information

Let \mathcal{X} and \mathcal{Y} be Euclidean spaces and let P_{XY} be a probability measure on the space $\mathcal{X} \times \mathcal{Y}$. Here, P_X and P_Y define the marginal probability measures. Similar to Suhov et al. [2016], for given function $(x, y) \in \mathcal{X} \times \mathcal{Y} \mapsto \varphi(x, y) \geq 0$, the Adaptive Mutual Information (AMI), denoted by $I_\varphi(X; Y)$, is defined as

$$I_\varphi(X; Y) = \mathbb{E}_{P_X P_Y} \left[\varphi(X, Y) g \left(\frac{dP_{XY}}{dP_X P_Y} \right) \right], \quad (1)$$

where $\frac{dP_{XY}}{dP_X P_Y}$ is the Radon-Nikodym derivative, and $g : (0, \infty) \mapsto \mathbb{R}$ is a convex function and $g(1) = 0$. Note that when $\frac{dP_{XY}}{dP_X P_Y} \rightarrow 1$ then $I_\varphi \rightarrow 0$. Let \mathcal{X} , \mathcal{Y} and \mathcal{Z} be Euclidean spaces and let P_{XYZ} be a probability measure on the space $\mathcal{X} \times \mathcal{Y} \times \mathcal{Z}$. We presume $P_{XY|Z}$, $P_{X|Z}$, and $P_{Y|Z}$ are the joint and marginal conditional probability measures, respectively. P_Z defines the marginal probability measure on the space \mathcal{Z} . Following Suhov et al. [2016], the Adaptive Conditional Mutual Information (ACMI), denoted by $I_\varphi(X; Y|Z)$, is defined as

$$I_\varphi(X; Y|Z) = \mathbb{E}_{P_Z P_{X|Z} P_{Y|Z}} \left[\varphi(X, Y, Z) g \left(\frac{dP_{XY|Z}}{dP_{X|Z} P_{Y|Z}} \right) \right]. \quad (2)$$

In this paper we focus on the particular case of $g(t) = \frac{(t-1)^2}{2(t+1)}$. Note that when $\varphi = 1$, the ACMI in (2) becomes the conditional geometric mutual information measure proposed in Yasaei Sekeh and Hero [2018]. Now we propose a hash-based estimator of the ACMI measure described below:

Hash-based Estimator of ACMI Consider N i.i.d samples $\{(X_i, Y_i, Z_i)\}_{i=1}^N$ drawn from P_{XYZ} . The dependence graph $G(X, Y, Z)$ is a directed multi-partite graph, consisting of three sets of nodes V , U , and W , with cardinalities denoted as $|V|$, $|U|$, and $|W|$, respectively and with the set of all edges E_G . The variable W here is different from the DNN weight matrix. Following similar arguments in Noshad et al. [2019], we map each point in the sets $\mathbf{X} = \{X_1, \dots, X_N\}$, $\mathbf{Y} = \{Y_1, \dots, Y_N\}$, and $\mathbf{Z} = \{Z_1, \dots, Z_N\}$ to the nodes in the sets U , V , and W , respectively, using the hash function H . Then let $H(x) = H_2(H_1(x))$, where the vector valued hash function $H_1 : \mathbb{R}^d \mapsto \mathbb{Z}^d$ is defined $H_1(x) = [h_1(x), \dots, h_1(x_d)]$, for $x = [x_1, \dots, x_d]$ and $h_1(x_i) = \lfloor \frac{x_i + b}{\epsilon} \rfloor$, for a fixed $\epsilon > 0$, and random variable $b \in [0, \epsilon]$. The random hash function $H_2 : \mathbb{Z}^d \mapsto \mathcal{F}$ is uniformly distributed on the output $\mathcal{F} = \{1, 2, \dots, F\}$ where for a fixed tunable integer c_H , $F = c_H N$. We define the following cardinality,

$$N_{ijk} = \#\{(X_t, Y_t, Z_t) \text{ s.t. } H(X_t) = i, H(Y_t) = j, H(Z_t) = k\}, \quad (3)$$

which is the number of joint collisions of the nodes (X_t, Y_t, Z_t) at the triple (v_i, u_j, ω_k) . Let N_{ik} , N_{jk} , and N_k be the number of collisions at the vertices (v_i, ω_k) , (u_j, ω_k) , and ω_k , respectively. By using N_{ijk} , N_{ik} , N_{jk} , and N_k , we define the following ratios,

$$r_{ijk} := \frac{N_{ijk}}{N}, \quad r_{ik} := \frac{N_{ik}}{N}, \quad r_{jk} := \frac{N_{jk}}{N}, \quad r_k := \frac{N_k}{N}. \quad (4)$$

Finally, substituting the above values into (2) we propose the following hash-based estimator of the ACMI measure, summed over all edges e_{ijk} of $G(X, Y, Z)$ having non-zero ratios:

$$\hat{I}_\varphi(X; Y|Z) = \sum_{e_{ijk} \in E_G} \varphi(i, j, k) \frac{r_{ik} r_{jk}}{r_k} g \left(\frac{r_{ijk} r_k}{r_{ik} r_{jk}} \right), \quad (5)$$

Theorem 1. For given $g(t) = \frac{(t-1)^2}{2(t+1)}$ and under the assumptions: **(A1)** The support sets \mathcal{X} , \mathcal{Y} , and \mathcal{Z} are bounded. **(A2)** The function φ is bounded. **(A3)** The continuous marginal, joint, and conditional density functions are belong to Hölder continuous class, Härdle [1990]. For fixed d_X , d_Y , and d_Z , as $n \rightarrow \infty$ we have

$$\widehat{I}_\varphi(X; Y|Z) \longrightarrow I_\varphi(X; Y|Z), \quad a.s. \quad (6)$$

The proof of Theorem 1 is given in the Supplementary Materials. Overall, X, Y, Z denote different sets of activations derived from groups of neurons in the algorithm and we obtain a scalar value as the outcome of the ACMI measure in (5). The flexibility in defining function φ offers a way to connect the probabilistic framework of mutual information to existing weight-based pruning approaches. In Section 4, we explore a variety of options for φ and empirically determine that a function defined on the weight matrix is the best possible formulation to achieve high pruning performance.

3.3 Procedure to Define Upper Pruning Limit of Layers

To help reduce the amount of manual effort required to gauge the upper pruning limit of each layer in a DNN, we propose a set of operating constraints to automate the process. Our approach is based on thresholds defined over the degradation in the quality of activations when a layer is pruned to various extents. First, we pose the desired overall compression percentage of the DNN, τ , as the sum of upper pruning limits of every layer, denoted by $\gamma^{(l)}$, in the DNN, $\tau = \sum_{l=1}^L \gamma^{(l)}$. To find $\gamma^{(l)}$, first, we collect the performance of an SVM model that is trained on activations from a layer, before it was pruned, and tested on activations collected after the layer was pruned to a desired percentage c . Here, the performance of the SVM model for a given layer l is denoted by $\alpha_c^{(l)}$. We collect the performance of the layer at different values of c . Once all the performances are collected, we create a subset of layers in the DNN that can be maximally compressed, denoted by M . The subset of layers in M are identified as those layers which contain performances in the top 80%, regardless of the compression percentage at which this performance is achieved. For all layers in M , we set $\gamma^{(l)}$ to be the largest pruning percentage that maintains the performance of the layer above random for a given dataset. The upper pruning limits for the remaining set of layers are computed based on a threshold over all the evaluated performances in the DNN, α , subject to the constraint on τ . We provide all the γ values used in the experiments in the supplementary materials.

3.4 Sensitivity of Filters

A common assumption made during pruning is that all filters in a layer have the same downstream impact and hence can be characterized solely on the magnitude of their weights. However, taking into account each filter’s impact on succeeding layers is an effective tool to assess their importance and protect information flow to important filters from being reduced by pruning. We define a sensitivity criteria, $\lambda(F_i^{l+1})$, that can be used to sort filters in their order of importance. Using this, we curate a subset of filters that are critical and hence need to be protected from pruning while the remaining filters are pruned using the steps in Alg. 1. To evaluate the sensitivity of filters in layer $l + 1$, we look at the weight matrix of it’s downstream layer $l + 2$, $W^{(l+2)}$, and assess the contributions from filters in $l + 1$ to those in $l + 2$. Here, $W^{(l+2)} \in \mathbb{R}^{N^{(l+2)} \times N^{(l+1)} \times H \times W}$, where H, W are the height and width of the filters in layer $l + 2$. For a given filter, the sum of normalized contributions across all the filters in $l + 2$ is the overall sensitivity, $\lambda(F_i^{l+1})$. It is defined as,

$$\lambda(F_i^{l+1}) = \sum_{f_c=1}^{N^{(l+2)}} \widetilde{W}^{(l+2)}(f_c, i) / \mathcal{C}^{(l+2)}(f_c), \quad \text{where } \mathcal{C}^{(l+2)}(f_c) = \sum_{f_p=1}^{N^{(l+1)}} \widetilde{W}^{(l+2)}(f_c, f_p). \quad (7)$$

Here, $\mathcal{C}^{(l+2)}$ is the normalization constant used to relate the weights of filters from $l + 1$ contributing to the same filter in $l + 2$ and $\widetilde{W}^{(l+2)}$ is the weight matrix of $l + 2$ averaged over the height and width. Once we obtain the order of sensitivity values for filters in a given layer, we define a threshold of highly sensitive filters that remain un-pruned. This is critical to ensure that sensitive filters which contribute a majority of the information downstream remain untouched. This in turn can help improve the overall compression performance since less sensitive filters can be pruned more without compromising the quality of information flowing between layers. Then, we apply the procedure of defining upper pruning limits for layers in a DNN and observe the degradation in performance

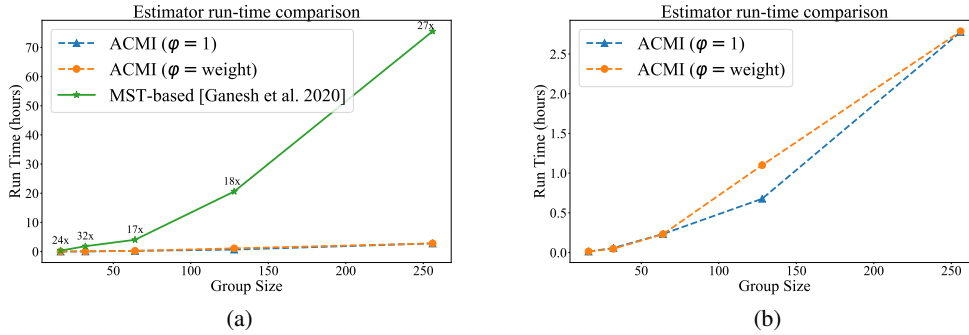


Figure 2: (2a) When comparing run-times between the MST-based estimator used in Ganesh et al. [2020] and our hash-based ACMI estimator, our estimator provides over $17\times$ speedup in run-time. (2b) Across different versions of our estimator, the run-times scale similarly as G increases.

relative to the case when all filters are pruned. Using this comparison, we fix the percentage of highly sensitive filters to remain un-pruned and only provide the set of relatively insensitive filters to Alg. 1.

4 Experimental Results

Dataset-DNN setup We use three standard Dataset-DNN architecture combinations to evaluate and compare our approach to standard baselines. They are, CIFAR10 [Krizhevsky et al., 2009]-VGG16 [Simonyan and Zisserman, 2015], CIFAR10-ResNet56 [He et al., 2016] and ILSVRC2012 [Russakovsky et al., 2015]-ResNet50. A detailed breakdown of each dataset and the experimental setup used in each experiment is included in the Supplementary Materials.

Metric Throughout the experiments, we use *run-time* to compare speed of estimators, *Compression* (%) as the primary metric to indicate the quality of a method while *Test Accuracy* (%) indicates the final testing set accuracy after compression and *Memory* (Mb) highlights the amount of memory consumed to store the weight matrices in “CSR” format. A high quality method must have high compression performance while maintaining a test accuracy higher than the nearest baseline.

4.1 Evaluation of Estimator

Run-time Comparison In SNACS, we use our ACMI estimator to compute the connectivity scores. MINT [Ganesh et al., 2020] is the closest existing method which uses a Minimum Spanning Tree (MST)-based conditional mutual information (CMI) estimator [Yasaei Sekeh and Hero, 2018]. To highlight the key practical differences between the MST-based and hash-based CMI estimators first we provide a comparison of run-time vs. group size across convolution layer 9 in VGG16. For this experiment, we use three distinct estimators, the MST-based estimator from MINT, our ACMI estimator with $\varphi = 1$ and $\varphi = \text{weight}$. Here, weight values are re-scaled between $[0, 1]$. From Fig. 2 we make two important observations, 1) **run-time increases with an increase in group-size across both estimators**, and 2) **relative to the run-time from the MST-based estimator, our estimator is faster by upwards of $17\times$** . Thus, we show that our estimator significantly reduces the overall run-time required to compute CMIs across a DNN.

Selection of φ There are number of potential functions we can associate with φ . In Table 1, we illustrate the top-4 functions, w.r.t. the compression ratio, across the VGG16-CIFAR10 experimental setup. We provide the entire list of functions explored in the Supplementary Materials. We observe that **all the performances listed in Table 1 outperform MINT**. Further, the combination of weight-based φ and our ACMI enhances the overall performance consistently. Since we find that $\varphi = \exp(\frac{-\text{weights}^2}{2})$ performs the best we set this as the default φ throughout the remaining experiments.

4.2 Large-scale Comparison

When compared to existing pruning methods that follow the train-prune-retrain pipeline, from Table 2 we observe that SNACS outperforms the current best baselines by a significant margin. We **improve**

Table 1: We compare the performance of a variety of φ functions (only top-4 shown here) and find that $\varphi = \exp(\frac{-\text{weights}^2}{2})$ performs the best. We use this in all the remaining experiments

φ function	Compression (%)	Test Accuracy (%)
constant = 1	84.02	93.53
weights	84.12	93.44
weights ²	84.17	93.58
$\exp(\frac{-\text{weights}^2}{2})$	84.46	93.51

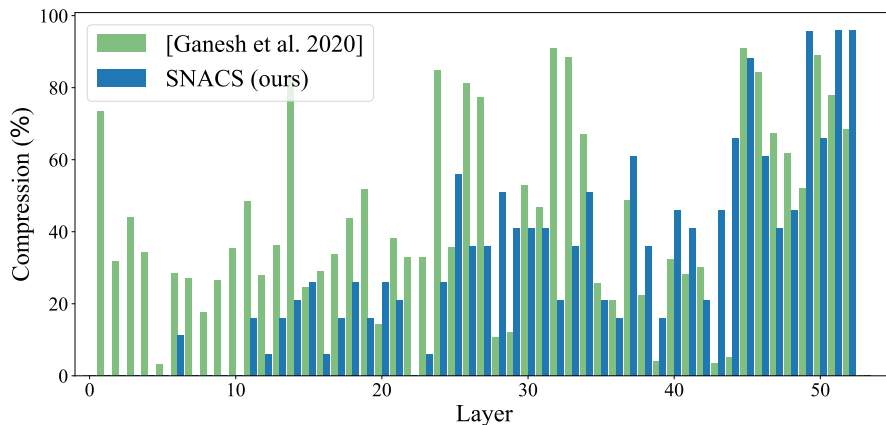
Table 2: Using a single train-prune-retrain cycle, SNACS easily outperforms prior baselines across all the Dataset-DNN architecture combinations. The order of baselines is based on Compression (%)

	Method	Compression(%)	Test Accuracy(%)	Memory(Mb)
VGG16 CIFAR-10	Baseline	N.A.	93.98	53.904
	Li et al. [2017]	64.00	93.40	N.A.
	Huang and Wang [2018]	73.80	93.02	N.A.
	Lin et al. [2019]	82.20	93.42	N.A.
	Ganesh et al. [2020]	83.46	93.43	9.020
	SNACS (ours)	84.45	93.51	8.622
ResNet56 CIFAR-10	Baseline	N.A.	92.55	3.110
	Lin et al. [2019]	11.80	93.38	N.A.
	Li et al. [2017]	13.70	93.06	N.A.
	Yu et al. [2018]	42.40	93.01	N.A.
	Wen et al. [2016]	43.50	93.29	N.A.
	Ganesh et al. [2020]	55.39	93.02	1.462
SNACS (ours)	62.96	93.13	1.234	
ResNet50 ILSVRC2012	Baseline	N.A.	76.13	91.163
	Lin et al. [2019]	16.86	71.95	N.A.
	Wen et al. [2016]	25.68	73.55	N.A.
	Huang and Wang [2018]	27.05	74.18	N.A.
	Luo et al. [2017]	51.45	71.01	N.A.
	Ganesh et al. [2020]	49.62	71.05	46.931
SNACS (ours)	51.95	72.56	45.002	

over not only Compression (%) but observe a boost in Test Accuracy that isn't common at such high sparsity levels. Apart from the boost in performance offered by the estimator itself, we look into the patterns of $\gamma^{(l)}$ obtained from our setup and compare it to MINT to gain further insight into how SNACS functions. From Fig. 3a and its extensions in the Supplementary Material, we observe that our approach yields a **distinct and consistent pattern of pruning that is applicable over all Dataset-DNN combinations** while there are no explicit patterns in pruning for MINT. We find that DNNs are more forgiving of pruning layers closer to the output than input since the retraining phase allows them to overcome the loss of abstract concepts learned in later layers but not fundamental structures when compressing the earlier layers of the network. Thus, in general we can automatically set γ values for all layers of a DNN, regardless of the dataset, while maintaining Test Accuracy.

4.3 Sensitivity-based Pruning

To highlight the impact of using sensitivity, we apply our sensitivity criterion to the CIFAR10-VGG16 experimental setup. Figs. 3b and 3c illustrate the impact of protecting a few sensitive filters from pruning in convolutional layers 4 and 9 in VGG16. This encourages an overall improvement in the compression (%) of layers that use sensitivity. Further, this approach is **applicable to layers that are closer to the input and the output**. In VGG16, by protecting sensitive filters in convolutional layers 4, 5, 8, 9 and 12 we are able to improve the overall compression (%) while maintaining performance. Results are provided in Table 3. With the use of a normalization constant across the contributions of each filter, the scale of all the λ values is maintained the same, however, the distribution of λ



(a) Compression per layer comparison for ILSVRC2012-ResNet50

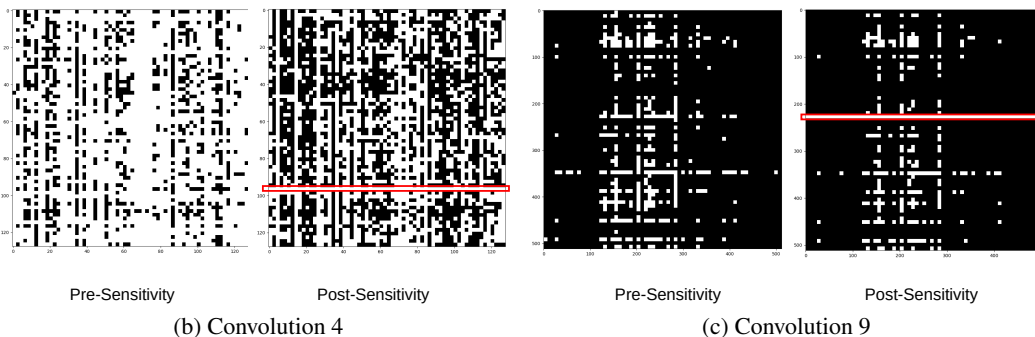


Figure 3: **(Top)** On observing the compression performance per layer in the ILSVRC2012-ResNet50 experiment, our method develops a consistent pattern of maximally pruning the later layers while minimally pruning the early layers. There is no such generic pattern in Ganesh et al. [2020]. **(Bottom)** Illustrations of filters retained (white) and pruned (black) pre- and post-sensitivity based pruning. Sparsely pruned early layers and densely pruned later layers can be pruned further when a sensitive subset of filters are protected (red highlight).

Table 3: By saving a small percentage of sensitive filters, we can further improve the overall Compression % while maintaining the Test Accuracy

	Method	Compression(%)	Test Accuracy(%)	Memory(Mb)
VGG16	Baseline	N.A.	93.98	53.904
	SNACS (ours)	84.45	93.51	8.622
CIFAR-10	SNACS + sensitivity (ours)	85.03	93.49	8.317

values vary depending on the position of the layer. Early layers contain λ values that mimic a normal distribution while the latter layers do not conform to any specific pattern. Empirical details of the experiment as well as the graphs for λ values are provided in the Supplementary Materials.

5 Conclusion

Overall, we propose a novel DNN pruning algorithm called SNACS which uses ACMI to measure the connectivity between filters, a simple set of operating constraints to automate the definition of upper pruning limits of layers in a DNN and a sensitivity criterion that helps protect a subset of critical filters from pruning. SNACS provides a faster overall run-time and improves accuracy in the estimation process, offers state-of-the-art levels of compression using a single train-prune-retrain cycle while the sensitivity criterion can be used to further boost the compression performance. An

important direction of future work is to extend this algorithm to an iterative approach and implement it during training time. Doing so would help reduce the overall training time while maintaining the strong test time impact of our approach.

6 Broader Impact

There are three main issues that affect the direct application of DNNs to real-world problems, large run-times during inference, and extensive memory usage. These constraints are critical in modern real-world applications like autonomous driving [Bechtel et al., 2018, Fridman et al., 2017, Nurvitadhi et al., 2017] and medical diagnosis [Lee et al., 2017, Abdel-Zaher and Eldeib, 2016, Anirudh et al., 2016], to name a few. Our pruning method solves these issues by offering a high compression rate which in turn reduces the overall number of computations as well as the memory required to store the DNN. While every key component in our experimental pipeline, sensitivity, constraints used to set the upper pruning limit of layers and measurement of connectivity between filters, is extendable to a DNN with alternative downstream tasks there is one possible issue that we do not account for, robustness to adversarial attacks [Kurakin et al., 2016, Goodfellow et al., 2015]. This is an extremely desirable property when DNNs are deployed in the real-world, especially in security applications. In our setup, the protection of sensitive filters and reduction in redundant information should help reduce its susceptibility to adversarial attacks since they often target the noisy and weak features. However, more work is required to adequately tackle and solve this problem.

7 Acknowledgements

This work has been partially supported (Madan Ravi Ganesh and Jason J. Corso) by NSF IIS 1522904 and NIST 60NANB17D191 and (Dawsin Blanchard and Salimeh Yasaei Sekeh) by NSF 1920908; the findings are those of the authors only and do not represent any position of these funding bodies.

References

- Ahmed M Abdel-Zaher and Ayman M Eldeib. Breast cancer classification using deep belief networks. *Expert Systems with Applications*, 46:139–144, 2016.
- Rushil Anirudh, Jayaraman J Thiagarajan, Timo Bremer, and Hyojin Kim. Lung nodule detection using 3d convolutional neural networks trained on weakly labeled data. In *Medical Imaging 2016: Computer-Aided Diagnosis*, volume 9785, page 978532. International Society for Optics and Photonics, 2016.
- Michael G Bechtel, Elise McElhiney, Minje Kim, and Heechul Yun. Deeppicar: A low-cost deep neural network-based autonomous car. In *2018 IEEE 24th International Conference on Embedded and Real-Time Computing Systems and Applications (RTCSA)*, pages 11–21. IEEE, 2018.
- Bin Dai, Chen Zhu, Baining Guo, and David Wipf. Compressing neural networks using the variational information bottleneck. In *International Conference on Machine Learning*, pages 1135–1144, 2018.
- Lex Fridman, Daniel E Brown, Michael Glazer, William Angell, Spencer Dodd, Benedikt Jenik, Jack Terwilliger, Julia Kindelsberger, Li Ding, Sean Seaman, et al. Mit autonomous vehicle technology study: Large-scale deep learning based analysis of driver behavior and interaction with automation. *arXiv preprint arXiv:1711.06976*, 1, 2017.
- Trevor Gale, Erich Elsen, and Sara Hooker. The state of sparsity in deep neural networks. *arXiv preprint arXiv:1902.09574*, 2019.
- Madan Ravi Ganesh, Jason J Corso, and Salimeh Yasaei Sekeh. Mint: Deep network compression via mutual information-based neuron trimming. *arXiv preprint arXiv:2003.08472*, 2020.
- Ian J. Goodfellow, Jonathon Shlens, and Christian Szegedy. Explaining and harnessing adversarial examples. In *3rd International Conference on Learning Representations, ICLR 2015, San Diego, CA, USA, May 7-9, 2015, Conference Track Proceedings*, 2015.

- Jiatao Gu, Graham Neubig, Kyunghyun Cho, and Victor OK Li. Learning to translate in real-time with neural machine translation. In *Proceedings of the 15th Conference of the European Chapter of the Association for Computational Linguistics: Volume 1, Long Papers*, pages 1053–1062, 2017.
- Song Han, Jeff Pool, John Tran, and William Dally. Learning both weights and connections for efficient neural network. In *Advances in neural information processing systems*, pages 1135–1143, 2015.
- Wolfgang Härdle. *Applied Nonparametric Regression*. Cambridge University Press, 1990.
- Kaiming He, Xiangyu Zhang, Shaoqing Ren, and Jian Sun. Deep residual learning for image recognition. In *2016 IEEE Conference on Computer Vision and Pattern Recognition (CVPR)*. IEEE, jun 2016. doi: 10.1109/cvpr.2016.90. URL <https://doi.org/10.1109%2Fcvpr.2016.90>.
- Zehao Huang and Naiyan Wang. Data-driven sparse structure selection for deep neural networks. In *Proceedings of the European conference on computer vision (ECCV)*, pages 304–320, 2018.
- Ye Jia, Ron J Weiss, Fadi Biadsy, Wolfgang Macherey, Melvin Johnson, Zhifeng Chen, and Yonghui Wu. Direct speech-to-speech translation with a sequence-to-sequence model. *Proc. Interspeech 2019*, pages 1123–1127, 2019.
- Alex Krizhevsky, Geoffrey Hinton, et al. Learning multiple layers of features from tiny images. 2009.
- Alexey Kurakin, Ian Goodfellow, and Samy Bengio. Adversarial examples in the physical world. *arXiv preprint arXiv:1607.02533*, 2016.
- Vadim Lebedev and Victor Lempitsky. Fast convnets using group-wise brain damage. In *Proceedings of the IEEE Conference on Computer Vision and Pattern Recognition*, pages 2554–2564, 2016.
- Yann LeCun, John S Denker, and Sara A Solla. Optimal brain damage. In *Advances in neural information processing systems*, pages 598–605, 1990.
- June-Goo Lee, Sanghoon Jun, Young-Won Cho, Hyunna Lee, Guk Bae Kim, Joon Beom Seo, and Namkug Kim. Deep learning in medical imaging: general overview. *Korean journal of radiology*, 18(4):570–584, 2017.
- Hao Li, Asim Kadav, Igor Durdanovic, Hanan Samet, and Hans Peter Graf. Pruning filters for efficient convnets. In *5th International Conference on Learning Representations, ICLR 2017, Toulon, France, April 24-26, 2017, Conference Track Proceedings*, 2017.
- Shaohui Lin, Rongrong Ji, Chenqian Yan, Baochang Zhang, Liujuan Cao, Qixiang Ye, Feiyue Huang, and David Doermann. Towards optimal structured cnn pruning via generative adversarial learning. In *Proceedings of the IEEE Conference on Computer Vision and Pattern Recognition*, pages 2790–2799, 2019.
- Zhuang Liu, Jianguo Li, Zhiqiang Shen, Gao Huang, Shoumeng Yan, and Changshui Zhang. Learning efficient convolutional networks through network slimming. In *Proceedings of the IEEE International Conference on Computer Vision*, pages 2736–2744, 2017.
- Zhuang Liu, Mingjie Sun, Tinghui Zhou, Gao Huang, and Trevor Darrell. Rethinking the value of network pruning. In *International Conference on Learning Representations*, 2018.
- Jian-Hao Luo and Jianxin Wu. An entropy-based pruning method for cnn compression. *arXiv preprint arXiv:1706.05791*, 2017.
- Jian-Hao Luo, Jianxin Wu, and Weiyao Lin. Thinet: A filter level pruning method for deep neural network compression. In *Proceedings of the IEEE international conference on computer vision*, pages 5058–5066, 2017.
- Morteza Noshad, Yu Zeng, and Alfred O Hero. Scalable mutual information estimation using dependence graphs. In *Proceedings of the IEEE International Conference on Acoustics, Speech and Signal Processing*, 2019.

- Eriko Nurvitadhi, Ganesh Venkatesh, Jaewoong Sim, Debbie Marr, Randy Huang, Jason Ong Gee Hock, Yeong Tat Liew, Krishnan Srivatsan, Duncan Moss, Suchit Subhaschandra, et al. Can fpgas beat gpus in accelerating next-generation deep neural networks? In *Proceedings of the 2017 ACM/SIGDA International Symposium on Field-Programmable Gate Arrays*, pages 5–14, 2017.
- Olga Russakovsky, Jia Deng, Hao Su, Jonathan Krause, Sanjeev Satheesh, Sean Ma, Zhiheng Huang, Andrej Karpathy, Aditya Khosla, Michael Bernstein, Alexander C. Berg, and Li Fei-Fei. ImageNet Large Scale Visual Recognition Challenge. *International Journal of Computer Vision (IJCV)*, 115(3):211–252, 2015. doi: 10.1007/s11263-015-0816-y.
- Karen Simonyan and Andrew Zisserman. Very deep convolutional networks for large-scale image recognition. In *3rd International Conference on Learning Representations, ICLR 2015, San Diego, CA, USA, May 7-9, 2015, Conference Track Proceedings*, 2015.
- Yuri Suhov, Izabella Stuhl, Salimeh Yasaei Sekeh, and Mark Kelbert. Basic inequalities for weighted entropies. *Aequationes mathematicae*, 90(4):817–848, 2016.
- Wei Wen, Chunpeng Wu, Yandan Wang, Yiran Chen, and Hai Li. Learning structured sparsity in deep neural networks. In *Advances in neural information processing systems*, pages 2074–2082, 2016.
- Salimeh Yasaei Sekeh and Alfred O Hero. Geometric estimation of multivariate dependency. *Entropy (Special Issue on Women in Information Theory)*, 21(8):787–841, 2018.
- Jaehong Yoon and Sung Ju Hwang. Combined group and exclusive sparsity for deep neural networks. In *Proceedings of the 34th International Conference on Machine Learning-Volume 70*, pages 3958–3966. JMLR. org, 2017.
- Ruichi Yu, Ang Li, Chun-Fu Chen, Jui-Hsin Lai, Vlad I Morariu, Xintong Han, Mingfei Gao, Ching-Yung Lin, and Larry S Davis. Nisp: Pruning networks using neuron importance score propagation. In *Proceedings of the IEEE Conference on Computer Vision and Pattern Recognition*, pages 9194–9203, 2018.

Appendix A Bounds on AMI

Recall the definition of AMI (Eqn. 1 in main paper). For the particular case of $g, g(t) = \frac{(t-1)^2}{2(t+1)}$, we have

$$I_\varphi(X; Y) = \frac{1}{2} \mathbb{E}_{P_X P_Y} \left[\varphi(X, Y) \left(\frac{dP_{XY}}{dP_X P_Y} + 1 \right) \right] - 2 \mathbb{E}_{P_X P_Y} \left[\varphi(X, Y) h \left(\frac{dP_{XY}}{dP_X P_Y} \right) \right], \quad (8)$$

where $h(t) = \frac{t}{t+1}$. When $\frac{dP_{XY}}{dP_X P_Y} = 1$, then the minimum value of I_φ is zero. Further, when P_{XY} and $P_X P_Y$ have no overlapping space then the second term in (8) becomes zero. Therefore, bounds on I_φ is given as,

$$0 \leq I_\varphi(X, Y) \leq \frac{1}{2} \mathbb{E}_{P_X P_Y} \left[\varphi(X, Y) \left(\frac{dP_{XY}}{dP_X P_Y} + 1 \right) \right]. \quad (9)$$

Appendix B Proof of Theorem 1

Recall our estimator (5) in Section 3.2,

$$\hat{I}_\varphi(X; Y|Z) = \sum_{e_{ijk} \in E_G} \varphi(i, j, k) \alpha_{ijk} g \left(\frac{r_{ijk}}{\alpha_{ijk}} \right), \quad (10)$$

where $\alpha_{ijk} = \frac{r_{ik} r_{jk}}{r_k}$. The expectation of \hat{I}_φ is derived as

$$\begin{aligned} \mathbb{E} \left[\hat{I}_\varphi(X; Y|Z) \right] &= \mathbb{E} \left[\sum_{e_{ijk} \in E_G} \varphi(i, j, k) \alpha_{ijk} g \left(\frac{r_{ijk}}{\alpha_{ijk}} \right) \middle| E_G \right] \\ &= \sum_{e_{ijk} \in E_G} \mathbb{E} \left[\varphi(i, j, k) \alpha_{ijk} g \left(\frac{r_{ijk}}{\alpha_{ijk}} \right) \middle| E_{ijk} \right], \end{aligned} \quad (11)$$

where E_{ijk} is the event that there is an edge between the vertices v_i, u_j , and ω_k . Let hash function H_1 maps the N i.i.d points X_k, Y_k , and Z_k to \tilde{X}_k, \tilde{Y}_k , and \tilde{Z}_k . Following notations in Noshad et al. [2019], denote E_i^{-1} be the event that there is exactly one vector from \tilde{X}_i that maps to v_i using H_2 . Define E_j^{-1} and E_k^{-1} similarly. Denote $E_{ijk}^{-1} := E_i^{-1} \cap E_j^{-1} \cap E_k^{-1}$ and let $\overline{E_{ijk}^{-1}}$ be complement set of E_{ijk}^{-1} .

We split the second line in equation (11) into two biases: without collision and due to collision, therefore based on the law of total expectation we have

$$\begin{aligned} &\sum_{e_{ijk} \in E_G} P(E_{ijk}^{-1} | E_{ijk}) \mathbb{E} \left[\varphi(i, j, k) \alpha_{ijk} g \left(\frac{r_{ijk}}{\alpha_{ijk}} \right) \middle| E_{ijk}^{-1}, E_{ijk} \right] \\ &+ \sum_{e_{ijk} \in E_G} P(\overline{E_{ijk}^{-1}} | E_{ijk}) \mathbb{E} \left[\varphi(i, j, k) \alpha_{ijk} g \left(\frac{r_{ijk}}{\alpha_{ijk}} \right) \middle| \overline{E_{ijk}^{-1}}, E_{ijk} \right]. \end{aligned} \quad (12)$$

First Step - Bias on w/o collision:

Similar to Lemma 7.3 in Noshad et al. [2019], we derive that

$$P(E_{ijk}^{-1} | E_{ijk}) = 1 - O \left(\frac{1}{\epsilon^d N} \right), \quad d = d_X + d_Y + d_Z. \quad (13)$$

This is because all three $|V|, |U|$, and $|W|$ are upper bounded by $O(\epsilon^{-d})$. Note that ϵ is a function of N . Additionally from Noshad et al. [2019] we infer the following results:

$$\mathbb{E}[\alpha_{ijk}] = \frac{\mathbb{E}[r_{ik}] \mathbb{E}[r_{jk}]}{\mathbb{E}[r_k]} + O \left(\sqrt{\frac{1}{N}} \right), \quad (14)$$

Note that (14) is implied based on the fact that $\mathbb{V}(\alpha_{ijk}) \leq O(1/N)$ which is proved by applying Efron-Stein inequality under assumptions **(A1)** and **(A3)**, similar to arguments in Lemma 7.10 from Noshad et al. [2019]. In addition, we have

$$\mathbb{E} \left[\frac{r_{ijk}}{\alpha_{ijk}} \right] = \frac{\mathbb{E}[r_{ijk}]}{\mathbb{E}[\alpha_{ijk}]} + O \left(\sqrt{\frac{1}{N}} \right), \quad (15)$$

$$\mathbb{E} \left[\frac{r_{ijk}}{\alpha_{ijk}} \right] = P(E_{ijk}^{\leq 1}) \mathbb{E} \left[\frac{r_{ijk}}{\alpha_{ijk}} | E_{ijk}^{\leq 1} \right] + P(E_{ijk}^{> 1}) \mathbb{E} \left[\frac{r_{ijk}}{\alpha_{ijk}} | E_{ijk}^{> 1} \right], \quad (16)$$

where by using similar arguments in (56) from Noshad et al. [2019], we have $P(E_{ijk}^{\leq 1}) = 1 - O(\sqrt{1/(\epsilon^d N)})$, therefore $P(E_{ijk}^{> 1}) = O(\sqrt{1/(\epsilon^d N)})$. Further the second term in (16) is the bias because of collision of H which will be proved in *Second step* in sequel that is upper bounded by $O(\sqrt{1/(\epsilon^d N)})$.

Let x_D and x_C respectively denote the discrete and continuous components of the vector x , with dimensions d_D and d_C . Also let $f_{X_C}(x_C)$ and $p_{X_D}(x_D)$ respectively denote density and pmf functions of these components associated with the probability measure P_X . Let X has d_C and d_D , Y has d'_C, d'_D , and Z has d''_C, d''_D continuous and discrete components, respectively. Then it can be shown that

$$\begin{aligned} & \mathbb{E}[r_{ijk} | E_{ijk}^{\leq 1}] \\ &= P(X_D = x_D, Y_D = y_D, Z_D = z_D) \epsilon^{d_C + d'_C + d''_C} (f(x_C, y_C, z_C | x_D, y_D, Z_D) + \Delta(\epsilon, q, \gamma)), \end{aligned} \quad (17)$$

where densities have bounded derivatives up to the order $q \geq 0$ and belong to the Hölder continuous class with smoothness parameter γ . Note that $\Delta(\epsilon, q, \gamma) \rightarrow 0$ as $N \rightarrow \infty$. Now from (50), (51), and (53) in Noshad et al. [2019] and from (14) and (15) above, under assumptions **(A1)** and **(A3)**, we derive that

$$\mathbb{E} \left[\frac{r_{ijk}}{\alpha_{ijk}} | E_{ijk}^{\leq 1} \right] = \frac{dP_{XYZ} P_Z}{dP_{XZ} P_{YZ}} + \tilde{\Delta}(\epsilon, q, \gamma) + O \left(\sqrt{\frac{1}{N}} \right), \quad (18)$$

where $H(x) = i, H(y) = j, H(z) = k$, and as $N \rightarrow \infty, \tilde{\Delta}(\epsilon, q, \gamma) \rightarrow 0$.

Second Step - Bias because of collision:

Let $\tilde{\mathbf{X}} = \{\tilde{X}_i\}_{i=1}^{L_X}$, $\tilde{\mathbf{Y}} = \{\tilde{Y}_i\}_{i=1}^{L_Y}$, $\tilde{\mathbf{Z}} = \{\tilde{Z}_i\}_{i=1}^{L_Z}$ respectively denote distinct outputs of H_1 with the N i.i.d points X_k, Y_k, Z_k as inputs. Denote $L_{XYZ} := |\tilde{\mathbf{X}} \cup \tilde{\mathbf{Y}} \cup \tilde{\mathbf{Z}}|$, $L_{XZ} := |\tilde{\mathbf{X}} \cup \tilde{\mathbf{Z}}|$, and $L_{YZ} := |\tilde{\mathbf{Y}} \cup \tilde{\mathbf{Z}}|$. In this step of the proof, we discuss the bias caused by the collision of H_1 that is the second line in (12):

$$\begin{aligned} \mathbb{B}_\varphi &:= \sum_{e_{ijk} \in E_C} P(\overline{E_{ijk}^{\leq 1}} | E_{ijk}) \mathbb{E} \left[\varphi(i, j, k) \alpha_{ijk} g \left(\frac{r_{ijk}}{\alpha_{ijk}} \right) | \overline{E_{ijk}^{\leq 1}}, E_{ijk} \right] \\ &\leq \sum_{i, j, k \in \mathcal{F}} P(E_{ijk}^{> 1}) \mathbb{E} \left[\mathbf{1}_{E_{ijk}} \varphi(i, j, k) \alpha_{ijk} g \left(\frac{r_{ijk}}{\alpha_{ijk}} \right) | E_{ijk}^{> 1} \right] \end{aligned} \quad (19)$$

where

$$E_{ijk}^{> 1} = E_i^{> 1} \cap E_j^{> 1} \cap E_k^{> 1},$$

and $E_i^{> 1}$ is the event that there are at least two vectors from \tilde{X}_i that map to v_i using H_2 . One again use the law of total expectation, then the RHS of (19) equals to

$$\begin{aligned} & \sum_{i, j, k \in \mathcal{F}} P(E_{ijk}^{> 1}) \left(P(E_{ijk} | E_{ijk}^{> 1}) \mathbb{E} \left[\varphi(i, j, k) \alpha_{ijk} g \left(\frac{r_{ijk}}{\alpha_{ijk}} \right) | E_{ijk}^{> 1}, E_{ijk} \right] \right. \\ & \quad \left. + P(\overline{E_{ijk}^{\leq 1}} | E_{ijk}^{> 1}) \mathbb{E} \left[\varphi(i, j, k) \alpha_{ijk} g \left(\frac{r_{ijk}}{\alpha_{ijk}} \right) | E_{ijk}^{> 1}, \overline{E_{ijk}^{\leq 1}} \right] \right) \\ &= \sum_{i, j, k \in \mathcal{F}} P(E_{ijk}) P(E_{ijk}^{> 1} | E_{ijk}) \mathbb{E} \left[\varphi(i, j, k) \alpha_{ijk} g \left(\frac{r_{ijk}}{\alpha_{ijk}} \right) | E_{ijk}^{> 1}, E_{ijk} \right] \end{aligned} \quad (20)$$

The equality in (20) is obtained based on Bayes error and $g = 0$ on the event $\overline{E_{ijk}}$. Now recall (13), so from (9), we bound the last line in (20) by

$$O\left(\frac{1}{\epsilon^d N}\right) \sum_{i,j,k \in \mathcal{F}} P(E_{ijk}) \mathbb{E} \left[\varphi(i, j, k) (r_{ijk} + \alpha_{ijk}) | E_{ijk}^{>1}, E_{ijk} \right]. \quad (21)$$

This implies that

$$\begin{aligned} \mathbb{B}_\varphi &\leq O\left(\frac{1}{\epsilon^d N}\right) \sum_{i,j,k \in \mathcal{F}} P(E_{ijk}) \left(\mathbb{E} \left[\varphi(i, j, k) r_{ijk} | E_{ijk}^{>1}, E_{ijk} \right] + \mathbb{E} \left[\varphi(i, j, k) \alpha_{ijk} | E_{ijk}^{>1}, E_{ijk} \right] \right) \\ &= O\left(\frac{1}{\epsilon^d N^2}\right) \sum_{i,j,k \in \mathcal{F}} P(E_{ijk}) \left(\mathbb{E} \left[\varphi(i, j, k) N_{ijk} | E_{ijk}^{>1}, E_{ijk} \right] + \mathbb{E} \left[\varphi(i, j, k) \frac{N_{ik} N_{jk}}{N_k} | E_{ijk}^{>1}, E_{ijk} \right] \right) \\ &= O\left(\frac{1}{\epsilon^d N^2}\right) \sum_{\tilde{\mathbf{x}}, \tilde{\mathbf{y}}, \tilde{\mathbf{z}}} p_{\tilde{\mathbf{X}}, \tilde{\mathbf{Y}}, \tilde{\mathbf{Z}}}(\tilde{\mathbf{x}}, \tilde{\mathbf{y}}, \tilde{\mathbf{z}}) \sum_{i,j,k \in \mathcal{F}} P(E_{ijk}) \\ &\quad \left(\mathbb{E} \left[\varphi(i, j, k) N_{ijk} | E_{ijk}^{>1}, E_{ijk}, \tilde{\mathbf{X}} = \tilde{\mathbf{x}}, \tilde{\mathbf{Y}} = \tilde{\mathbf{y}}, \tilde{\mathbf{Z}} = \tilde{\mathbf{z}} \right] \right. \\ &\quad \left. + \mathbb{E} \left[\varphi(i, j, k) \frac{N_{ik} N_{jk}}{N_k} | E_{ijk}^{>1}, E_{ijk}, \tilde{\mathbf{X}} = \tilde{\mathbf{x}}, \tilde{\mathbf{Y}} = \tilde{\mathbf{y}}, \tilde{\mathbf{Z}} = \tilde{\mathbf{z}} \right] \right) \end{aligned} \quad (22)$$

Define

$$\begin{aligned} \mathcal{A}_{ijk} &:= \left\{ r : H_2(\tilde{X}_r) = i, H_2(\tilde{Y}_r) = j, H_2(\tilde{Z}_r) = k \right\}, \quad \mathcal{A}_k := \left\{ r : H_2(\tilde{Z}_r) = k \right\} \\ \mathcal{A}_{ik} &:= \left\{ r : H_2(\tilde{X}_r) = i, H_2(\tilde{Z}_r) = k \right\}, \quad \mathcal{A}_{jk} := \left\{ r : H_2(\tilde{Y}_r) = j, H_2(\tilde{Z}_r) = k \right\}. \end{aligned} \quad (23)$$

Let M_r , be the number of the input points $(\mathbf{X}, \mathbf{Y}, \mathbf{Z})$ mapped to $(\tilde{X}_r, \tilde{Y}_r, \tilde{Z}_r)$. Therefore for i, j, k we can rewrite N_{ijk} as

$$N_{ijk} = \sum_{r=1}^{L_{XYZ}} \mathbb{1}_{\mathcal{A}_{ijk}}(r) M_r. \quad (24)$$

Similarly M'_r, \widetilde{M}_s , and \overline{M}_t are defined the number of the input points mapped to $(\tilde{X}_r, \tilde{Z}_r), (\tilde{Y}_s, \tilde{Z}_s)$, and \tilde{Z}_t , respectively and we can write

$$N_{ik} = \sum_{r=1}^{L_{XZ}} \mathbb{1}_{\mathcal{A}_{ik}}(r) M'_r, \quad N_{jk} = \sum_{s=1}^{L_{YZ}} \mathbb{1}_{\mathcal{A}_{jk}}(s) \widetilde{M}_s, \quad N_k = \sum_{t=1}^{L_Z} \mathbb{1}_{\mathcal{A}_k}(t) \overline{M}_t. \quad (25)$$

Under the assumption that φ is bounded, we have

$$\begin{aligned} \mathbb{B}_\varphi &\leq O\left(\frac{1}{\epsilon^d N^2}\right) \sum_{\tilde{\mathbf{x}}, \tilde{\mathbf{y}}, \tilde{\mathbf{z}}} p_{\tilde{\mathbf{X}}, \tilde{\mathbf{Y}}, \tilde{\mathbf{Z}}}(\tilde{\mathbf{x}}, \tilde{\mathbf{y}}, \tilde{\mathbf{z}}) \sum_{i,j,k \in \mathcal{F}} P(E_{ijk}) \\ &\quad \left(\sum_{r=1}^{L_{XYZ}} P\left(r \in \mathcal{A}_{ijk} | E_{ijk}^{>1}, E_{ijk}, \tilde{\mathbf{X}} = \tilde{\mathbf{x}}, \tilde{\mathbf{Y}} = \tilde{\mathbf{y}}, \tilde{\mathbf{Z}} = \tilde{\mathbf{z}}\right) \mathbb{E} \left[M_r | E_{ijk}^{>1}, E_{ijk}, \tilde{\mathbf{X}} = \tilde{\mathbf{x}}, \tilde{\mathbf{Y}} = \tilde{\mathbf{y}}, \tilde{\mathbf{Z}} = \tilde{\mathbf{z}} \right] \right. \\ &\quad \left. + \sum_{r=1}^{L_{XZ}} \sum_{s=1}^{L_{YZ}} \sum_{t=1}^{L_Z} P\left(r \in \mathcal{A}_{ik}, s \in \mathcal{A}_{jk}, t \in \mathcal{A}_k | E_{ijk}^{>1}, E_{ijk}, \tilde{\mathbf{X}} = \tilde{\mathbf{x}}, \tilde{\mathbf{Y}} = \tilde{\mathbf{y}}, \tilde{\mathbf{Z}} = \tilde{\mathbf{z}}\right) \right. \\ &\quad \left. \mathbb{E} \left[\frac{M'_r \widetilde{M}_s}{\overline{M}_t} | E_{ijk}^{>1}, E_{ijk}, \tilde{\mathbf{X}} = \tilde{\mathbf{x}}, \tilde{\mathbf{Y}} = \tilde{\mathbf{y}}, \tilde{\mathbf{Z}} = \tilde{\mathbf{z}} \right] \right), \end{aligned} \quad (26)$$

Next we find the probability terms:

$$P\left(r \in \mathcal{A}_{ijk} | E_{ijk}^{>1}, E_{ijk}, \tilde{\mathbf{X}} = \tilde{\mathbf{x}}, \tilde{\mathbf{Y}} = \tilde{\mathbf{y}}, \tilde{\mathbf{Z}} = \tilde{\mathbf{z}}\right) = \frac{P\left(r \in \mathcal{A}_{ijk}, E_{ijk}^{>1} | \tilde{\mathbf{X}} = \tilde{\mathbf{x}}, \tilde{\mathbf{Y}} = \tilde{\mathbf{y}}, \tilde{\mathbf{Z}} = \tilde{\mathbf{z}}\right)}{P\left(E_{ijk}^{>1} | \tilde{\mathbf{X}} = \tilde{\mathbf{x}}, \tilde{\mathbf{Y}} = \tilde{\mathbf{y}}, \tilde{\mathbf{Z}} = \tilde{\mathbf{z}}\right)}. \quad (27)$$

Let us find the denominator of (27) first. Define $a = 1$ when $i = j = k$ and $a = 3$ for the case $i \neq j \neq k$:

$$\begin{aligned} & P\left(E_{ijk}^{>1} | \tilde{\mathbf{X}} = \tilde{\mathbf{x}}, \tilde{\mathbf{Y}} = \tilde{\mathbf{y}}, \tilde{\mathbf{Z}} = \tilde{\mathbf{z}}\right) \\ &= 1 - P\left(E_{ijk}^{=0} | \tilde{\mathbf{X}} = \tilde{\mathbf{x}}, \tilde{\mathbf{Y}} = \tilde{\mathbf{y}}, \tilde{\mathbf{Z}} = \tilde{\mathbf{z}}\right) - P\left(E_{ijk}^{=1} | \tilde{\mathbf{X}} = \tilde{\mathbf{x}}, \tilde{\mathbf{Y}} = \tilde{\mathbf{y}}, \tilde{\mathbf{Z}} = \tilde{\mathbf{z}}\right) \\ &= 1 - \left(\frac{F-a}{F}\right)^{L_{XYZ}} - \left(\frac{L_{XYZ}}{F^a} \left(\frac{F-a}{F}\right)^{L_{XYZ}-a}\right) = O\left(\frac{L_{XYZ}^2}{F^{a+1}}\right) \end{aligned} \quad (28)$$

Further

$$\begin{aligned} & P\left(r \in \mathcal{A}_{ijk}, E_{ijk}^{>1} | \tilde{\mathbf{X}} = \tilde{\mathbf{x}}, \tilde{\mathbf{Y}} = \tilde{\mathbf{y}}, \tilde{\mathbf{Z}} = \tilde{\mathbf{z}}\right) \\ &= P\left(r \in \mathcal{A}_{ijk} | E_{ijk}^{>1}, \tilde{\mathbf{X}} = \tilde{\mathbf{x}}, \tilde{\mathbf{Y}} = \tilde{\mathbf{y}}, \tilde{\mathbf{Z}} = \tilde{\mathbf{z}}\right) P\left(r \in \mathcal{A}_{ijk} | \tilde{\mathbf{X}} = \tilde{\mathbf{x}}, \tilde{\mathbf{Y}} = \tilde{\mathbf{y}}, \tilde{\mathbf{Z}} = \tilde{\mathbf{z}}\right) \\ &= \left(1 - \left(\frac{F-a}{F}\right)^{L_{XYZ}-a}\right) \left(\frac{1}{F}\right)^a = O\left(\frac{L_{XYZ}}{F^{a+1}}\right) \end{aligned} \quad (29)$$

Combining (28) and (29) yields

$$P\left(r \in \mathcal{A}_{ijk} | E_{ijk}^{>1}, E_{ijk}, \tilde{\mathbf{X}} = \tilde{\mathbf{x}}, \tilde{\mathbf{Y}} = \tilde{\mathbf{y}}, \tilde{\mathbf{Z}} = \tilde{\mathbf{z}}\right) = O\left(\frac{1}{L_{XYZ}}\right). \quad (30)$$

Now we simplify the following term:

$$P\left(r \in \mathcal{A}_{ik}, s \in \mathcal{A}_{jk}, t \in \mathcal{A}_k | E_{ijk}^{>1}, E_{ijk}, \tilde{\mathbf{X}} = \tilde{\mathbf{x}}, \tilde{\mathbf{Y}} = \tilde{\mathbf{y}}, \tilde{\mathbf{Z}} = \tilde{\mathbf{z}}\right). \quad (31)$$

First assume that $\tilde{X}_v \neq \tilde{Y}_v \neq \tilde{Z}_v$ for $v = r, s, t$. Then

$$\begin{aligned} & P\left(r \in \mathcal{A}_{ik}, s \in \mathcal{A}_{jk}, t \in \mathcal{A}_k | E_{ijk}^{>1}, E_{ijk}, \tilde{\mathbf{X}} = \tilde{\mathbf{x}}, \tilde{\mathbf{Y}} = \tilde{\mathbf{y}}, \tilde{\mathbf{Z}} = \tilde{\mathbf{z}}\right) \\ &\leq P\left(r \in \mathcal{A}_{ik} | E_{ik}^{>1}, \tilde{\mathbf{X}} = \tilde{\mathbf{x}}, \tilde{\mathbf{Y}} = \tilde{\mathbf{y}}, \tilde{\mathbf{Z}} = \tilde{\mathbf{z}}\right) P\left(s \in \mathcal{A}_{jk} | E_{jk}^{>1}, \tilde{\mathbf{X}} = \tilde{\mathbf{x}}, \tilde{\mathbf{Y}} = \tilde{\mathbf{y}}, \tilde{\mathbf{Z}} = \tilde{\mathbf{z}}\right) \\ &\quad P\left(t \in \mathcal{A}_k | E_k^{>1}, \tilde{\mathbf{X}} = \tilde{\mathbf{x}}, \tilde{\mathbf{Y}} = \tilde{\mathbf{y}}, \tilde{\mathbf{Z}} = \tilde{\mathbf{z}}\right) = O\left(\frac{1}{L_{XZ}L_{YZ}L_Z}\right). \end{aligned} \quad (32)$$

Next assume that $\tilde{X}_v = \tilde{Y}_v = \tilde{Z}_v$ for $v = r, s, t$, therefore $H_2(\tilde{X}_v) = H_2(\tilde{Y}_v) = H_2(\tilde{Z}_v)$, for $v = r, s, t$. Then

$$P\left(r \in \mathcal{A}_{ik}, s \in \mathcal{A}_{jk}, t \in \mathcal{A}_k | E_{ijk}^{>1}, E_{ijk}, \tilde{\mathbf{X}} = \tilde{\mathbf{x}}, \tilde{\mathbf{Y}} = \tilde{\mathbf{y}}, \tilde{\mathbf{Z}} = \tilde{\mathbf{z}}\right) = \delta_{ijk} O\left(\frac{1}{L_{XYZ}}\right), \quad (33)$$

By using equations (33), (32), and (30) in (26) we obtain an upper bound on bias with collision:

$$\begin{aligned} \mathbb{B}_\varphi &\leq O\left(\frac{1}{\epsilon^d N^2}\right) \sum_{\tilde{\mathbf{x}}, \tilde{\mathbf{y}}, \tilde{\mathbf{z}}} p_{\tilde{\mathbf{X}}, \tilde{\mathbf{Y}}, \tilde{\mathbf{Z}}}(\tilde{\mathbf{x}}, \tilde{\mathbf{y}}, \tilde{\mathbf{z}}) \sum_{i,j,k \in \mathcal{F}} P(E_{ijk}) \\ &\quad \left(O\left(\frac{1}{L_{XYZ}}\right) \sum_{r=1}^{L_{XYZ}} \mathbb{E}\left[M_r | E_{ijk}^{>1}, E_{ijk}, \tilde{\mathbf{X}} = \tilde{\mathbf{x}}, \tilde{\mathbf{Y}} = \tilde{\mathbf{y}}, \tilde{\mathbf{Z}} = \tilde{\mathbf{z}}\right] \right. \\ &\quad \left. + \left(O\left(\frac{1}{L_{XZ}L_{YZ}L_Z}\right) + \delta_{ijk} O\left(\frac{1}{L_{XYZ}}\right)\right) \sum_{r=1}^{L_{XZ}} \sum_{s=1}^{L_{YZ}} \sum_{t=1}^{L_Z} \mathbb{E}\left[\frac{M'_r \tilde{M}_s}{\tilde{M}_t} | E_{ijk}^{>1}, E_{ijk}, \tilde{\mathbf{X}} = \tilde{\mathbf{x}}, \tilde{\mathbf{Y}} = \tilde{\mathbf{y}}, \tilde{\mathbf{Z}} = \tilde{\mathbf{z}}\right]\right) \\ &= O\left(\frac{1}{\epsilon^d N^2}\right) \sum_{\tilde{\mathbf{x}}, \tilde{\mathbf{y}}, \tilde{\mathbf{z}}} p_{\tilde{\mathbf{X}}, \tilde{\mathbf{Y}}, \tilde{\mathbf{Z}}}(\tilde{\mathbf{x}}, \tilde{\mathbf{y}}, \tilde{\mathbf{z}}) \sum_{i,j,k \in \mathcal{F}} P(E_{ijk}) \left(O\left(\frac{N}{L_{XYZ}}\right) + \left(O\left(\frac{N}{L_{XZ}L_{YZ}L_Z}\right) + \delta_{ijk} O\left(\frac{N}{L_{XYZ}}\right)\right)\right) \\ &= O\left(\frac{1}{\epsilon^d N^2}\right) \sum_{\tilde{\mathbf{x}}, \tilde{\mathbf{y}}, \tilde{\mathbf{z}}} p_{\tilde{\mathbf{X}}, \tilde{\mathbf{Y}}, \tilde{\mathbf{Z}}}(\tilde{\mathbf{x}}, \tilde{\mathbf{y}}, \tilde{\mathbf{z}}) \left(O\left(\frac{N}{L_{XYZ}}\right) + \left(O\left(\frac{N}{L_{XZ}L_{YZ}L_Z}\right) + O\left(\frac{1}{L_{XYZ}}\right)\right)\right) \mathbb{E}\left[\sum_{i,j,k \in \mathcal{F}} \mathbf{1}_{E_{ijk}}\right] \\ &\leq O\left(\frac{1}{\epsilon^d N^2}\right) \sum_{\tilde{\mathbf{x}}, \tilde{\mathbf{y}}, \tilde{\mathbf{z}}} p_{\tilde{\mathbf{X}}, \tilde{\mathbf{Y}}, \tilde{\mathbf{Z}}}(\tilde{\mathbf{x}}, \tilde{\mathbf{y}}, \tilde{\mathbf{z}}) \left(O\left(\frac{N}{L_{XYZ}}\right) + \left(O\left(\frac{N}{L_{XZ}L_{YZ}L_Z}\right) + O\left(\frac{1}{L_{XYZ}}\right)\right)\right) L_{XYZ} \\ &\leq O\left(\frac{1}{\epsilon^d N}\right). \end{aligned} \quad (34)$$

Hence as $N \rightarrow \infty$, the bias estimator due to collision tends to zero i.e. $\mathbb{B}_\varphi \rightarrow 0$.

Third Step - Denote N'_{ijk} , N'_{ik} , N'_{jk} , and N'_k respectively are the number of the input points $(\mathbf{X}, \mathbf{Y}, \mathbf{Z})$, (\mathbf{X}, \mathbf{Z}) , (\mathbf{Y}, \mathbf{Z}) , and \mathbf{Z} mapped to the buckets $(\tilde{X}_i, \tilde{Y}_j, \tilde{Z}_k)$, $(\tilde{X}_i, \tilde{Z}_k)$, $(\tilde{Y}_j, \tilde{Z}_k)$, and \tilde{Z}_k using H_1 . Define the notations $r(i) = H_2^{-1}(i)$ for $i \in \mathcal{F}$ and $s(x) := H_1(x)$ for $x \in \mathcal{X} \cup \mathcal{Y} \cup \mathcal{Z}$. Then from (18), we have

$$\mathbb{E} \left[\frac{N'_{s(X)s(Y)s(Z)} N'_{s(Z)}}{N'_{s(X)s(Z)} N'_{s(Y)s(Z)}} \right] = \frac{dP_{XYZ} P_Z}{dP_{XZ} P_{YZ}} + \tilde{\Delta}(\epsilon, q, \gamma) + O\left(\sqrt{\frac{1}{N}}\right). \quad (35)$$

We simplify the first term in (12) as

$$\begin{aligned} & \sum_{i,j,k \in \mathcal{F}} P(E_{ijk}^{\leq 1}) \mathbb{E} \left[\mathbb{1}_{E_{ijk}} \varphi(i, j, k) \alpha_{ijk} g\left(\frac{r_{ijk}}{\alpha_{ijk}}\right) \middle| E_{ijk}^{\leq 1} \right] \\ &= \left(1 - O\left(\frac{1}{\epsilon^d N}\right)\right) \sum_{i,j,k \in \mathcal{F}} \mathbb{E} \left[\mathbb{1}_{E_{ijk}} \varphi(i, j, k) \alpha_{ijk} g\left(\frac{r_{ijk}}{\alpha_{ijk}}\right) \middle| E_{ijk}^{\leq 1} \right] \\ &= \sum_{i,j,k \in \mathcal{F}} \mathbb{E} \left[\mathbb{1}_{E_{ijk}} \varphi(i, j, k) \frac{N_{ik} N_{jk}}{N_k N} g\left(\frac{N_{ijk} N_k}{N_{ik} N_{jk}}\right) \middle| E_{ijk}^{\leq 1} \right] + O\left(\frac{1}{\epsilon^d N}\right) \\ &= \sum_{i,j,k \in \mathcal{F}} \mathbb{E} \left[\mathbb{1}_{E_{ijk}} \varphi(r(i), r(j), r(k)) \frac{N'_{r(i)r(k)} N'_{r(j)r(k)}}{N'_{r(k)} N} g\left(\frac{N'_{r(i)r(j)r(k)} N'_{r(k)}}{N'_{r(i)r(k)} N'_{r(j)r(k)}}\right) \right] + O\left(\frac{1}{\epsilon^d N}\right). \end{aligned} \quad (36)$$

Denote

$$\beta(r(i), r(j), r(k)) = \frac{N'_{r(i)r(j)r(k)} N'_{r(k)}}{N'_{r(i)r(k)} N'_{r(j)r(k)}}.$$

Therefore the last line in (36) is equal to

$$\begin{aligned} &= \frac{1}{N} \sum_{i,j,k \in \mathcal{F}} \mathbb{E} \left[\varphi(r(i), r(j), r(k)) \frac{N'_{r(i)r(j)r(k)}}{\beta(r(i), r(j), r(k))} g\left(\beta(r(i), r(j), r(k))\right) \right] + O\left(\frac{1}{\epsilon^d N}\right) \\ &= \frac{1}{N} \mathbb{E} \left[\sum_{i=1}^N \frac{\varphi(s(X), s(Y), s(Z))}{\beta(s(X), s(Y), s(Z))} g\left(\beta(s(X), s(Y), s(Z))\right) \right] + O\left(\frac{1}{\epsilon^d N}\right), \end{aligned} \quad (37)$$

where

$$\beta(s(X), s(Y), s(Z)) = \frac{N'_{s(X)s(Y)s(Z)} N'_{s(Z)}}{N'_{s(X)s(Z)} N'_{s(Y)s(Z)}}.$$

The expression (37) equals:

$$\begin{aligned} &= \mathbb{E}_{P_{XYZ}} \left[\mathbb{E} \left[\frac{\varphi(s(X), s(Y), s(Z))}{\beta(s(X), s(Y), s(Z))} g\left(\beta(s(X), s(Y), s(Z))\right) \middle| \mathbf{X} = \mathbf{x}, \mathbf{Y} = \mathbf{y}, \mathbf{Z} = \mathbf{z} \right] \right] + O\left(\frac{1}{\epsilon^d N}\right) \\ &= \mathbb{E}_{P_{XYZ}} \left[\varphi(X, Y, Z) h\left(\frac{dP_{XYZ} P_Z}{dP_{XZ} P_{YZ}}\right) \right] + \tilde{\Delta}(\epsilon, q, \gamma) + O\left(\sqrt{\frac{1}{N}}\right) + O\left(\frac{1}{\epsilon^d N}\right), \end{aligned} \quad (38)$$

where $h(t) = g(t)/t$ and (38) is derived by borrowing Lemma 7.9 from Noshad et al. [2019]. Hence from (38) and (12), and the fact that $\tilde{\Delta}(\epsilon, q, \gamma) \rightarrow 0$ as $N \rightarrow \infty$, we conclude

$$\mathbb{E} \left[\hat{I}_\varphi(X; Y|Z) \right] \rightarrow \mathbb{E}_{P_{XYZ}} \left[\varphi(X, Y, Z) h\left(\frac{dP_{XYZ} P_Z}{dP_{XZ} P_{YZ}}\right) \right], \text{ as } N \rightarrow \infty. \quad (39)$$

This completes the proof.

Appendix C Validating the Estimator

In this section we validate the MSE performance of the estimator proposed in SNACS across varying size of dimensionality and the number of total samples.

Setup In order to observe the performance of the estimator when the number of samples are varied, we set the dimensionality of X, Y to one and Z to two. This setup is used to mimic the dimensionality difference, at a small scale, in our experiments. We vary the number of samples in the range $\in \{500, 1000, 5000, 10000, 15000, 20000, 25000\}$. To observe the impact of a change in dimensionality on the estimator’s performance, we restrict the total number of samples to 5000 and varying the dimensions of X, Y, Z across $\{3, 10, 20, 30, 50\}$. In both the setups, we sample data from a multivariate normal distribution where the covariance matrix is set as the identity function and μ is zero.

Results Fig. 4 shows the results of our experiments where in Fig. 4a, we observe the steady decrease in MSE as the number of samples are increased. This matches our expectation of a good estimator where an increase in the number of samples improves the overall estimation accuracy and thus, reduces the MSE. Fig. 4b illustrates the steady increase in MSE when the number of samples are held constant but the dimensionality of the input variables grows larger. Further, the secondary curves where $\varphi = \exp(-\frac{\|act\|_2^2}{2})$ shows that the inclusion of this term improves the overall performance and matches the expected trends from a good estimator.

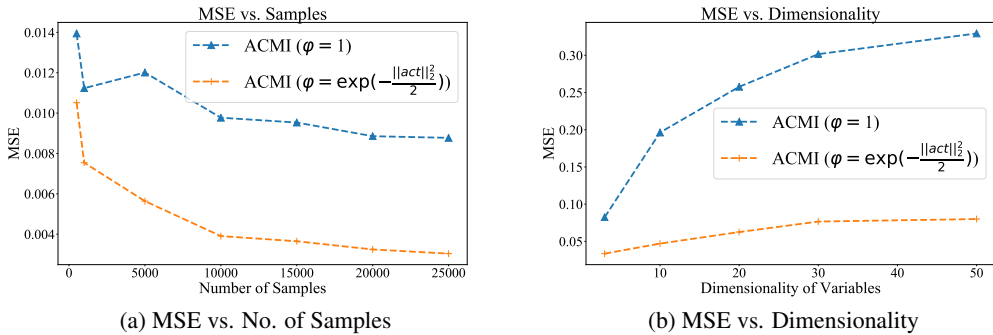


Figure 4: **(Fig. 4a)** An increase in the number of samples while dimensionality of input variables are held constant shows steadily decreasing MSE. **(Fig. 4b)** Increasing the dimensionality of input variables while the total number of samples are held constant shows a steady worsening of the MSE. Overall, the trends observed in both experiments match the expectations from a valid estimator.

Appendix D Dataset and Preprocessing

CIFAR10 This dataset is a 10 class subset of the original 80 million tiny images dataset. The dataset split contains 50000 images for training, split as 5000 images/class, and 10000 images for testing where there are 1000 images/class. Each image in the dataset is originally $32 \times 32 \times 3$. For preprocessing, we randomly crop the image after padding 4 pixels, then we randomly flip the image horizontally before normalizing its values using mean (0.4914, 0.4822, 0.4465) and std. (0.2470, 0.2435, 0.2616) for each channel respectively. During testing, the images are only normalized and provided to the DNN.

ILSVRC2012 This dataset contains 1000 different classes of images totalling to about 1.2 million images overall for training and 50000 images for validation. The number of images per class varies between 732 to 1300. For preprocessing, we randomly crop the image in to $224 \times 224 \times 3$, then we randomly flip the image horizontally before normalizing its values using mean (0.485, 0.456, 0.406) and std. (0.229, 0.224, 0.225) for each channel respectively. During testing, we resize the original image to $256 \times 256 \times 3$, take a center crop of size $224 \times 224 \times 3$ before normalizing them.

Appendix E Experimental Setup

Throughout the entire experimental results section, we use three major Dataset-DNN combinations, CIFAR10-VGG16, CIFAR10-ResNet56 and ILSVRC2012-ResNet50. Table 4 lists the main hyper-

parameters used to train the VGG16 and ResNet56 networks and obtain their baseline performances. Table 5 list the basic hyper-parameters used to retrain the VGG16, ResNet56 and ResNet50 networks and obtain their final performance.

Table 4: Training setups used to obtain pre-trained network weights

	VGG16	ResNet56
Epochs	300	300
Batch Size	128	128
Learning Rate	0.1	0.01
Schedule	90, 180, 260	150, 225
Optimizer	SGD	SGD
Weight Decay	0.0005	0.0002
Multiplier	0.2	0.1

Table 5: Base retraining setup used to obtain final performance listed in Table 1 of main paper

	VGG16	ResNet56	ResNet50
Epochs	300	300	130
Batch Size	128	128	64
Learning Rate	0.1	0.1	0.1
Schedule	[90, 180, 260]	[90, 180, 260]	[30, 60, 90, 100]
Optimizer	SGD	SGD	SGD
Weight Decay	0.0005	0.0002	0.0001
Multiplier	0.2	0.1	0.1

E.1 Procedure to Set Upper Pruning Limit of Layers

Across all the experiments, when using our set of operating constraints to define γ , we collect the performance of an SVM model across $c \in \{1, 6, 11, \dots, 96\}$.

E.2 Evaluation of Estimator

Run-Time To compare the improvement offered by our hash-based ACMI estimator, we choose the Minimum Spanning Tree-based (MST) CMI estimator from MINT [Ganesh et al., 2020] as the nearest competitive baseline. To ensure fair comparison, we use ACMI with $\varphi = 1$ as well as $\varphi = \text{weight}$ where weights are scaled to be between $[0, 1]$. We apply all the estimators over the 9^{th} convolution layer of VGG16 since it is the most dense layer available in the DNN. Here, we vary G values for both the layer l and $l + 1$ (8 and 9) over 16, 32, 64, 128 and 256. We use an average run-time from 10 trials, except for groups 128 and 256 for the MST-based estimator for which we use 2 trials. Most importantly, we set 200 samples per class which results in a total of 2000 samples of activations.

Selection of φ We implement a number of possible functions and evaluate them over the CIFAR10-VGG16 experimental setup. The exact hyper-parameters used to obtain ACMI values and obtain the final test accuracy are provided in Tables 5, 6 and 7. We maintain $G = 64$ throughout these experiments. The retraining parameters are based on the the compression (%) at which the model has a test accuracy that matches or exceeds 93.43% (from MINT).

E.3 Large Scale Comparison

The setup to obtain the final results presented in Table 2 of the main paper are presented under Tables 6 and 5. For VGG16 and ResNet50, $G = 64$ for all the layers in the network. For ResNet56, convolution layers up to 20 have $G = 16$ for l while convolution layers up to 19 have $G = 16$ for $l + 1$. Similarly, convolution layers between 21 and 38 have $G = 32$ for l while convolution layers between 20 and 37 have $G = 32$ for $l + 1$. The remaining layers have $G = 64$ for both l and $l + 1$

Table 6: Hyper-parameters specific to the φ function used final performance the best possible final performance $\geq 93.43\%$. Here, act refers to the activations

	1	weights	weights ²	$\exp(-\frac{\text{weights}^2}{2})$	$\ \text{act}\ _2$
δ	0.9865	0.9925	0.9925	0.988	0.995
$\gamma^{(1)}$	00.00	00.00	00.00	00.00	00.00
$\gamma^{(2)}$	00.00	00.00	00.00	00.00	00.00
$\gamma^{(3)}$	21.02	21.02	21.02	21.02	00.00
$\gamma^{(4)}$	51.02	51.02	51.02	51.02	96.02
$\gamma^{(5)}$	61.03	51.02	51.02	71.02	51.02
$\gamma^{(6)}$	86.03	91.01	91.01	86.03	96.02
$\gamma^{(7)}$	91.01	91.01	91.01	91.01	86.03
$\gamma^{(8)}$	91.01	91.01	91.01	91.01	91.01
$\gamma^{(9)}$	96.02	96.02	96.02	96.02	96.02
$\gamma^{(10)}$	91.01	91.01	91.01	91.01	91.01
$\gamma^{(11)}$	91.01	91.01	91.01	91.01	91.01
$\gamma^{(12)}$	66.01	66.01	66.01	66.01	61.03
$\gamma^{(13)}$	91.01	91.01	91.01	91.01	91.01
$\gamma^{(14)}$	00.00	00.00	00.00	00.00	00.00
Compression(%)	84.02	84.12	84.17	84.46	76.13

Table 7: Hyper-parameters specific to the φ function used setup used to obtain final performance listed in Table 1 of main paper. Here, act refers to the activations

	weights $\ \text{act}\ _2$	$\exp(-\frac{\text{weights}^2 \ \text{act}\ _2^2}{2})$
δ	0.880	0.919
$\gamma^{(1)}$	00.00	00.00
$\gamma^{(2)}$	00.00	00.00
$\gamma^{(3)}$	41.01	36.03
$\gamma^{(4)}$	56.03	61.03
$\gamma^{(5)}$	61.03	56.03
$\gamma^{(6)}$	81.03	86.03
$\gamma^{(7)}$	86.03	96.02
$\gamma^{(8)}$	91.01	86.03
$\gamma^{(9)}$	96.02	91.01
$\gamma^{(10)}$	96.02	96.02
$\gamma^{(11)}$	91.01	81.03
$\gamma^{(12)}$	61.03	71.02
$\gamma^{(13)}$	91.01	86.03
$\gamma^{(14)}$	00.00	00.00
Compression(%)	82.59	76.99

layers. We use the final compression per layer plots in subsequent sections as proxies for the γ values set in our experiments.

E.4 Sensitivity-based Pruning

When using sensitivity-based pruning for VGG16, we highlight convolution layers 4, 5, 8, 9 and 12 are the main layers where we can save sensitive filters and observe a gain in compression. In Table 8 we present the updated γ values for these layers when sensitivity is added. These γ values were obtained after applying our operating constraints on $c \in \{2, 4, \dots, 98\}$.

Table 8: Comparison of γ values for convolution layers 4,5,8,9 and 12 in VGG16 when sensitive filters are protected

	w/o Sensitivity	Sensitivity-based
δ	0.988	0.9879
$\gamma^{(3)}$	21.02	49.95
$\gamma^{(4)}$	51.02	55.39
$\gamma^{(7)}$	91.01	92.72
$\gamma^{(8)}$	91.01	93.77
$\gamma^{(11)}$	91.01	92.55
Compression(%)	84.45	85.03

Appendix F Additional Figures for Results

We provide the extended set of figures for compression per layer comparisons for the VGG16 and ResNet56 experiments. Further, we add the histogram plots for λ values.

Appendix G Discussion: Operating Constraints to Set Upper Pruning Limits

The operating constraints to help automatically set the upper pruning limits of layers in a DNN were formulated based on empirical observations on the degradation of activation quality when a layer is pruned. We observed that the activations from later layers in a DNN, which are known to learn more abstract concepts of the data, performed extremely well even when a simple SVM model is used to classify them. Secondly, the drop in their performance is slow with increasing compression. To easily highlight layers whose activations possess such characteristics, we use the top-80% threshold and prune them up to the maximum possible extent which maintains the performance above random. We observed through our own experiments and the precedents set in previous works that such layers can be pruned to large degrees yet the final test accuracy can be maintained after retraining.

The mid-layers possess activations that fall in quality quickly while the early layers often have activations with very weak performance. Hence, we use a simple threshold over all the performances collected since this simple statistic matches the amount of desired pruning that these layers can handle without an extreme drop in performance. We vary this simple threshold based on the overall constraint set for τ since they represent how pruning scales between layers yet they do NOT represent the absolute maximum that the layer can be pruned, individually.

Appendix H Complexity of SNACS

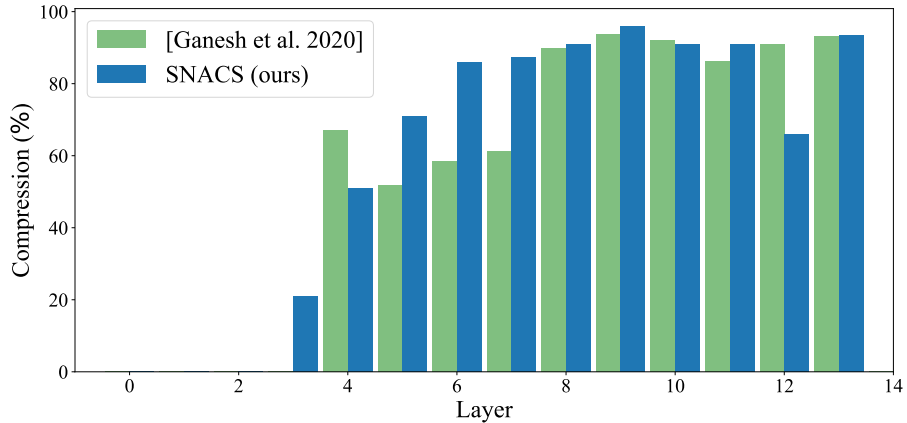
We breakdown the discussion on the computational complexity of SNACS into two distinct parts, 1) the complexity of the hash-based estimator, and 2) the complexity of Algorithm 1 in the main paper.

H.1 Complexity of hash-based estimator

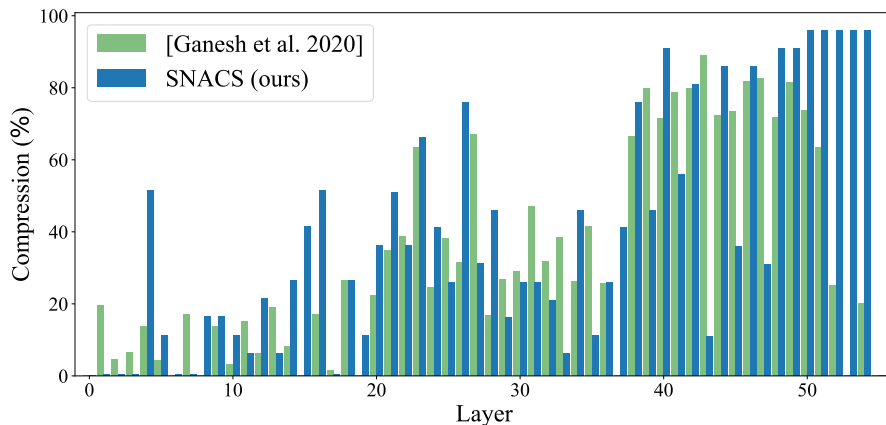
Extending the discussion provided in Noshad et al. [2019], we find that the estimation process is dependent on two main factors, the total number of samples, m , and the dimensionality of each sample. From the original paper, we find that the computational complexity is linearly dependent on the number of samples. Also, in our setup the dimensionality of a sample is capped by $\overline{F_j^{(l)}}$ which includes activations from all the filters in a layer excluding j . However, the estimator is still scales linearly with dimensionality.

H.2 Complexity of Algorithm 1

There are 2 primary factors which affect the time complexity of Algorithm 1 in the main paper, 1) the number of groups associated with layers l and $l + 1$, and 2) the total number of layers in the



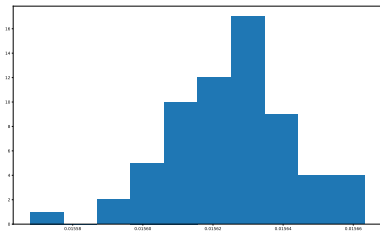
(a) Compression per layer comparison for CIFAR10-VGG16



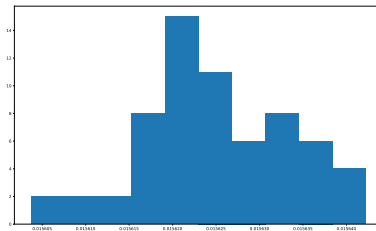
(b) Compression per layer comparison for CIFAR10-RESNET56

Figure 5: Across both VGG16 and ResNet56, we observe that our approach to setting γ works well. The later layers are pruned significantly more when compared to the early layers across all Dataset-DNN combinations.

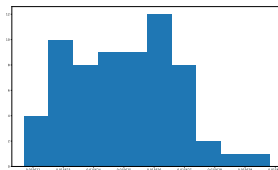
DNN. The double **FOR** loop has an upper bound of $\mathcal{O}(N^{(l)} N^{(l+1)})$ if the number of groups defined matches the number of filters in each layer. Practically, we have an upper bound of $\mathcal{O}(G^{(l)} G^{(l+1)})$. Overall, the algorithm itself is executed $L - 1$ times.



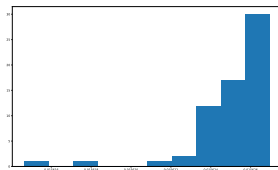
(a) Convolution 4



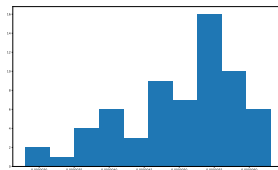
(b) Convolution 5



(c) Convolution 8



(d) Convolution 9



(e) Convolution 12

Figure 6: Comparison of the histogram of λ values between early layers (Conv. 4 and 5) and the later layers (Conv. 8, 9, 12). The early layers resemble normal distributions while the latter layers do not conform to a specific pattern.